Stability of big surface bubbles: impact of evaporation and bubble size

Jonas Miguet, Marina Pasquet, Florence Rouyer, Yuan Fang, Emmanuelle Rio

Stability of Big Surface Bubbles: Impact of Evaporation and Bubbles Size

Jonas Miguet[1], Marina Pasquet[1], Florence Rouyer [2], Yuan Fang [3], Emmanuelle Rio[1]

[1] Univ. Paris Sud, Laboratoire de Physique des Solides, CNRS UMR 8502
[2] Laboratoire Navier, Université Paris-Est, 77454 Marne-la-Vallée, France
[3] PepsiCo Global R&D, Valhalla, New York 10595, United States

July 6, 2022

Abstract

At the end of their life, surface bubbles burst and emit aerosols, which drastically impact exchanges in liquid as well as in pathogens or flavors with the surrounding atmosphere. This exchange depends on the thickness of the liquid film and is thus linked to the bubble drainage dynamics and to their lifetime. In this article, we propose to explore both feature for big surface bubbles depending on their size. We also explore the impact of atmospheric humidity by a careful control and systematic variation of the relative humidity. We show that a model including both capillary and gravity driven drainage gives a prediction of the bubble lifetime in line with experiments provided convection is taken into account to calculate the evaporation rate.

1 Introduction

Due to their wide range applicability, surface bubbles have attracted considerable attention is the past decades. The general reasons for this is their ubiquity and the enhanced transfer of materials from the liquid reservoir to the overlying atmosphere in their presence through the production of aerosols. In societal applications, studies may be found in different contexts: domestic [1], recreational [2], industrial [3]. Because surface active materials may adsorb at their surface during the ascent [4], the produced aerosols feature excess concentration of such materials, which has consequences in the release of flavours from fizzy drinks [5]. In a geophysical context, the aerosols produced by bursting bubbles at the surface of the oceans constitute a primary source [6] that influences clouds formation and their radiative properties [7]. They can also favour the transport of pathogens [8], which, in turn may alter the bubble stability [9].

Despite their vast range of applicability, numerous questions remain only poorly addressed in the literature. Generally speaking, two distinct mechanisms for the production of aerosols have been identified. Up to ten jet drops [10] can be produced upon the destabilisation of the curvature-induced jet that forms in the bubble cavity after the fast burst of the cap film [11]. In addition, hundreds of film drops can be formed during the disintegration of the cap film upon bursting [12]. The number of produced film drops, their size and ejection velocity depend on the film thickness, which in turn is linked both to the bubble lifetime and to the thinning dynamics of the thin liquid film. In the following, we detail the typical scenario along a surface bubble life: adoption of an equilibrium shape at the surface, thinning of the cap film, nucleation of a hole and subsequent bursting.

When a bubble emerges at a liquid/gas interface, a first regime of fast thinning of the bubble cap film proceeds until it adopts an equilibrium shape that is determined by the balance of buoyancy, that pulls the gas phase in the volume towards the atmosphere and the surface tension-induced force along the circular meniscus that binds it to the bath [13]. Therefore, a relevant dimensionless quantity to address the question of the shape of the bubble is the Bond number :

$$Bo = \frac{\rho_{\text{liq}} g R^2}{\gamma}, \tag{1}$$

where ρ_{liq} [kg.m^{-3}] and γ [N.m^{-1}] are respectively the density and the surface tension of the liquid (provided that the density of the gas may be neglected), g the acceleration due to gravity [m.s^{-2}], and R [m] the radius of the spherical cap of the bubble, above the meniscus. For pure viscous liquids, Debrégeas et al. [14] proposed a gravity driven flow with zero interfacial stress. The viscous film thickness on top of the bubble decays exponentially with a characteristic time related to the shape of the bubble [15, 16]. For liquids with surface active species, a metastable equilibrium is reached, where a surface tension gradient necessary to hold the weight of the film is established. A slower thinning mechanism develops, driven by capillary pressure and/or gravity, but also by evaporation [9]. A continuous transition from zero stress to zero velocity boundary condition (dependant on the relative strength of interfacial to bulk stresses) was

proposed by Bhamla *et al.* [17]. Champougny *et al.* [18] measured different thinning rates for different surfactant concentrations and proposed a model based on an intermediary boundary condition *ie* a slip length. Lhuissier *et al.* proposed a drainage model that will be discussed further, based on the coupling between a capillary driven flow localised at the foot of the bubble and the periodic emission of so called marginal regeneration plumes, as first reported by Mysels *et al.* [19]

Another potential contributor to thinning is evaporation, about which literature is much more scarce with only one recent paper to address its impact on the stability of surface bubbles [9]. However, the few systematic studies of the stability of thin films under controlled partial pressure of water in the gas phase, relative to the saturation pressure (*ie* relative humidity) report a strong impact of this parameter [20, 21, 22]. Bubble artists also invariably report decreasing stability of their films with decreasing humidity. On the other hand, when the evaporation rate get high enough, it can lead to Marangoni flows that can stabilise the bubble [23].

As the film thins, it becomes more and more prompt to nucleate a hole that expands quickly (typically milliseconds[24]) and irremediably leads to the destruction of the bubble. The process that initiates the rupture is not fully understood [25] but the stochastic nature of this event is well established by now [26, 27]. The total lifetime of the bubbles being the sum of both contribution (thinning and initiation of a hole), a sufficient characterisation of a given system can only be achieved with repeated measurements.

In this paper, we provide the first study of the stability of surface bubbles with a systematic variation of their size (here centimetric bubbles) in a controlled humidity environment. We benefit from an automated generation and measurement of the bubble lifetime to obtain good statistics (thousands of bubbles). We show that the characteristic time relevant to predict the bubble lifetime is given by the comparison between the drainage velocity and the evaporation rate.

2 Experimental methods

The physicochemichal system used for this study consists of ultrapure water (resistivity=18.2 M.Ω.m) to which 0.5 cmc (*ie* 0.62 g.L^{-1}) [28] of Tetradecyl Trimethyl Ammonium Bromide, thereafter referred to as TTAB, is added. The latter is purchased from Sigma-Alrich and is further purified through recrystalization [29]. It was indeed found that, at this low concentration, the interface is progressively polluted (likely by the traces of tetradecanol left after the original synthesis), which drastically lowers the equilibrium surface tension and therefore alters the reproductibility of the experiments.

The experimental set-up for the measurement of the bubbles lifetime is represented in figure 1. A cylindrical

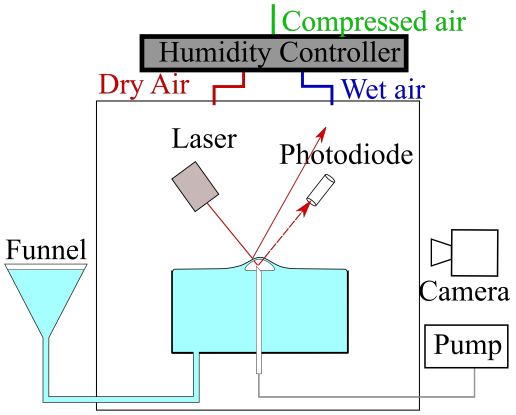

Figure 1: A container with the solution of interest is set in a humidity controlled chamber. The container is filled from the outside of the chamber, and the level of liquid is precisely controlled with a funnel, trough hydrostatic adjustment to ensure a proper laser alignment in absence of a bubble (dotted line). Air is injected by a pump to create the bubbles, the presence of which is assessed by the subsequent divergence of the laser beam with respect to the photodiode (solid line). Images are recorded from the side during the experiments.

container featuring a teflon ring in its upper end is used to facilitate the emergence of a meniscus above the level of the container and images of the bubbles (see figure 2b) are taken from the side with a monochrome camera (Marlin). A red laser beam (wave length and light power are respectively equal to of 650 nm and 5 mW) is directed to the center of the container, where the bubbles are created. In the absence of a bubble, the reflection of the beam on the interface is focused with a convex lens on a photodiode that emits a subsequent electric signal. When a bubble appears, the beam diverges and the photodiode is turned off. Making use of a python routine, this system allows for the repeated and automated generation of bubbles together with a measurement of bubbles lifetime. The whole set-up is set in a 75x45x45 cm^3 plexiglas chamber. A humidity sensor (SHT25) is placed a few centimeters away from the bubble in the container, on the same horizontal plane and coupled to a flow regulator. A PID controller determines whether the output flow of air passes directly to the chamber (dry air), or first through the bottom of a water bottle (humid air), which allows for the control of the humidity RH in the measuring chamber. The room is kept at a constant temperature of 22°C. In order to precisely control the level of the meniscus, the container is plugged to a funnel that is placed out of the box and which vertical position sets that of the meniscus making use of hydrostatic equilibrium. The images are taken at 4 frames per second and processed *a posteriori* making use of the scikit-image library in python. This provides an independent measurement of the bubbles lifetime, necessary to eliminate some

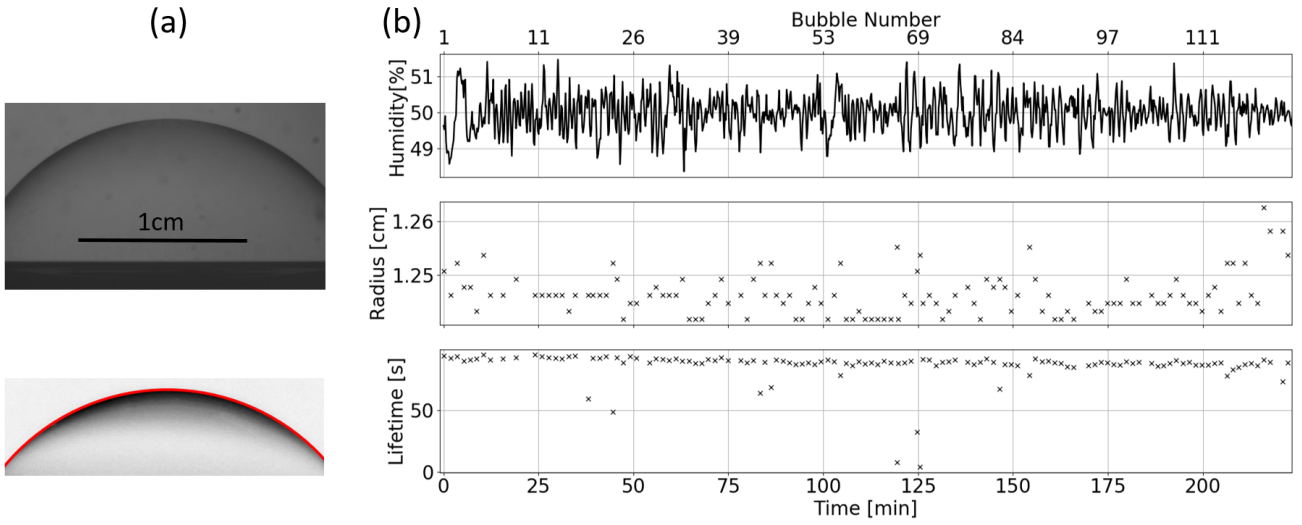

Figure 2: (a) Top: raw image of a bubble which spherical cap radius is 1.25 cm. Bottom: the same image after processing with scikit-image library in Python. The red arc of circle represents the optimal fit to the contour of the bubble and provides a measure of the radius of curvature of the cap.(b) Raw experimental data for eache bubble (top axis) along time (bottom axis). Top: humidity measured in the chamber. Middle: lifetime of the bubbles. Bottom: radius of the produced bubbles.

artefacts that can arise when daughter bubbles [30] or a loss of height caused by evaporation prevent the alignment of the laser with the photodiode. The size of every bubbles is also measured using this routine (figure 2a). For the injection of the bubbles, a PTFE tube of inner diameter 325 μm is guided trough a capillary tube to which it is hermetically glued, from the bottom of the container. The lower end of the PTFE tube is plugged to a solenoid valve that allows a flow of air triggered by a flow-controlled aquarium pump to blow bubbles when required, for a controlled amount of time.

Figure 2b represents the time evolution of the different parameters in the course of an experiment. The bottom axis indicates the time ellapsed since the onset of the set up, while the top axis displays the corresponding bubble number. The top chart indicates that the humidity is properly controlled within 1.5%. This is to compare with the accuracy of the humidity sensor, which is around 1.8 % below 90 %, around 2 % between 90 and 95 % and around 2.5% above 95 %. The accuracy of the humidity control and measurement is thus limited by the sensor and decreases with the humidity rate. The experiments conducted at high humidity (*ie* close to saturation) thus could not be as precisely controlled in terms of absolute humidity because the precision of the sensors drops and condensation could damage the electronic connections. Instead, humid air was continuously injected in the chambers, and condensation could be observed, while the few readings we took guaranteed values above 95%.

The middle chart in Figure 2 shows that, for a given injection time the size of the bubbles is reproducible ($\pm$ 40 μm). The bottom one shows that, for a given humidity in the chamber and a given bubble size, the bubbles lifetime does not vary significantly, which is necessary to assess an overall reliable significance of the measured lifetimes [23].

To provide more insight into these systems, the thickness evolution of film at the apex of the bubbles was measured using a reflectometric technique, described in more details in [18, 21]. These experiments were conducted in a closed chamber which humidity was controlled with another device described in [31].

3 Results and discussion

3.1 Results on the bubbles lifetime

All the collected data on the bubbles lifetimes are represented in figure 3 as a function of their size, for different humidity values. The stability of the bubbles increases significantly with their size for a given humidity. On the other hand, environmental humidity is demonstrated to play a crucial role in the stability of the bubbles. We indeed measured lifetime differences up to one order of magnitude for similar bubbles submitted to different relative humidity values. This effect is not linear since the stability increases approximately by a factor of 10 between 50% and saturated values, while it increases only by a factor of two between 20 % and 50 %. A closer insight into this phenomena was measured by fixing the bubble size to 1.3 cm and let the humidity in the chamber increase progressively starting from 65 % up to 99

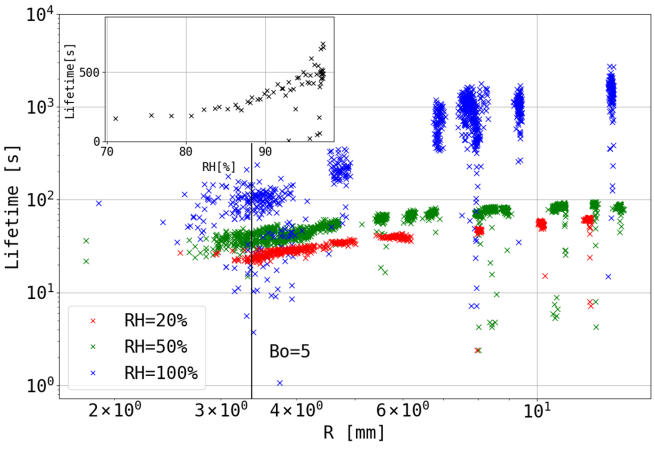

Figure 3: Raw data of bubbles lifetime as a function of their spherical cap radius of curvature for three different humidity values.

%(see the inset in figure 3).

In Figure 3, the dispersion of the data points seems to increase with the relative humidity. This may be due to the accuracy of the humidity captor, which decreases with RH, as mentioned in section 2.

3.2 Bubbles drainage

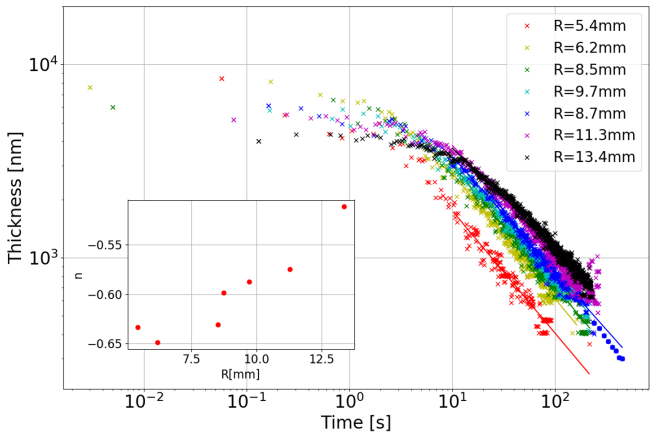

Figure 4: Thickness of bubbles film at the apex as a function of time, for various bubbles size, close to water vapor saturation. Full lines are the optimal fits using a power law with the exponent as a free parameter. The inset shows the dependency of this exponent with the bubbles size. The plain circles are obtained using the software NanoCalc to process the spectra.

In Figure 4, we show the evolution of the film thickness at the apex of the bubbles versus time for an environmental humidity close to saturation for different bubbles radii (corresponding to Bond number above 5). In this situation, in (almost complete) absence of evaporation, the two potential drivers for the thinning of the cap are capillary pressure and gravity. For pure solutions, it was shown that the transition between a capillary dominated regime (with a macroscopic driving force of $2\pi\gamma S/R$, where S[m^2] is the area of the bubble cap) and a gravity dominated regime (where the driving force is $4\pi R^3\rho_{\rm liq}g/3$) occurs for a Bond number of 0.25 [32]. Our systems is however qualitatively different because the presence of surfactants can induce a so-called marginal pinching in the vicinity of the bubble foot (that is, at the transition region between the meniscus and the overlaying cap). This pinch was proved by Aradian *et al.* [33] theoretically consistent with rigid boundary conditions at the surface of the films, while Howell *et al.* [34] demonstrated the impossibility for a film to pinch in the case of fully mobile interfaces. In the case of TTAB solutions, neither rigid nor mobile film thinning models would prove consistent with experimental observations [18]. However, an indirect proof of the existence of such pinching can be obtained through the observation of convective plumes, of smaller thickness, that rise from the bottom to the cap of the bubble. This phenomenon has been reported in numerous studies both in the case of vertical films [19, 35, 36] and bubbles [18, 12]. Lhuissier et. al[12] considered for the first time the influence of the pinch on the overall cap drainage dynamics. Featuring the smallest thickness (and therefore maximum viscous dissipation), the pinched zone is assumed to be limiting in the whole drainage process. The surface rigidity is ensured by assuming an accumulation of surfactants at the foot of the bubble, under the action of drainage of the cap, which creates a subsequent Marangoni stress. The instability that gives rise to the plumes is assumed to arise from this accumulation and the corresponding contribution to the thinning (by replacement of thick films portions by thin regeneration plumes), being dependent on the drainage driven accumulation of surfactants, is assumed to be of the same order of magnitude. Finally, considering that the thickness difference between the rising plumes and the mean cap thickness is of the same order than the cap thickness itself, they use scaling laws for the capillary flow in the limit of small bubbles within the pinch and the matching of the curvature of the cap with that of the pinch (see equation 5) to obtain the following prediction for the cap thickness [12]:

$$h \sim l_c \left(\frac{\eta l_c}{\gamma t}\right)^{2/3} \left(\frac{R}{l_c}\right)^{7/3}, \qquad (2)$$

where h[m] is the mean thickness of the spherical cap, η[kg.m^{-1}.s^{-}1] the bulk viscosity of the solution and l_c [m] the capillary length of the system defined as $\sqrt{\gamma/\rho_{\rm liq}g}$.

This predicts a scaling of the film thinning with time $h \sim t^{-2/3}$. On the other hand, in the case of large bubbles *ie* gravity driven flows, the thickness is expected to evolve as $t^{-1/2}$ whatever the boundary condition at the interfaces [17]. The data in Figure 4 indeed exhibit a n algebraic behavior with time after a few seconds and we

thus fitted the data by a power law. The extracted exponent is reported in the inset of Figure 4 and exhibits a transition from a $-2/3$ exponent for the smallest bubble to $-1/2$ for the largest, implying that both phenomena need to be taken into account for our experiment. Momentum conservation in the pinched area can be written using the Stokes equation, which scales as:

$$\eta \frac{V}{\delta^2} \sim \frac{\gamma}{Rl} + \rho_{\text{liq}} g, \tag{3}$$

where $V[\text{m.s}^{-1}]$ is the typical velocity of the fluid within the thickness of the film, $\delta[\text{m}]$ and $l[\text{m}]$ the two characteristic lengths of the pinch that are, respectively, its thickness and its tangential extension (with respect to the local bubble surface, see the inset of Figure 5). Mass conservation writes:

$$\frac{dh}{dt} + \frac{P}{S} hV \sim 0, \tag{4}$$

where $P[\text{m}]$ and $S[\text{m}^2]$ are repectively the perimeter of the (circular) meniscus and the surface area of the cap.

We now follow the same steps than Lhuissier *et al.* [12] for the closure of the problem in presence of gravity in equation 3. Matching the curvature of the cap with that of the pinch implies:

$$\frac{1}{R} \sim \frac{h - \delta}{l^2} \tag{5}$$

The thickness of the pinch is of the order of h and evolves in parallel with it, an affirmation confirmed by Nierstrasz [35] who finds a constant ratio δ/h of 0.2 during the whole draining process of a vertical foam film. Equation 5 allows to express l as the geometrical mean of the two other lengths of the problem, *ie* $l \sim \sqrt{Rh}$, so that:

$$V \sim \frac{\gamma}{\eta} \frac{h^{3/2}}{R^{3/2}} + \frac{\rho_{\text{liq}} g h^2}{\eta}, \tag{6}$$

where the first term in the right-hand side accounts for capillary suction and the second one for gravity driven drainage. Finally, we assume a large bubble limit for the geometrical factor in equation 4, namely: $P/S \sim 1/R$ in line with a Bond number larger than 5 [13]. The system of equations for the drainage is therefore closed and leaves us with the possibility of a numerical integration of equation 4, with V given by equation 6 and using h_0, the measured initial thickness, as an initial condition. Figure 5 illustrates the validity of this approach with three representative bubbles (for the sake of readability) taken from the same experiments as figure 4, when evaporation is negligible. Indeed the capillary model (dashed lines) underestimates the thinning velocity of the film as compared to the more complete model presented above that better describes our data. Of course the discrepancy between both models is more and more important as the bubble size increases.

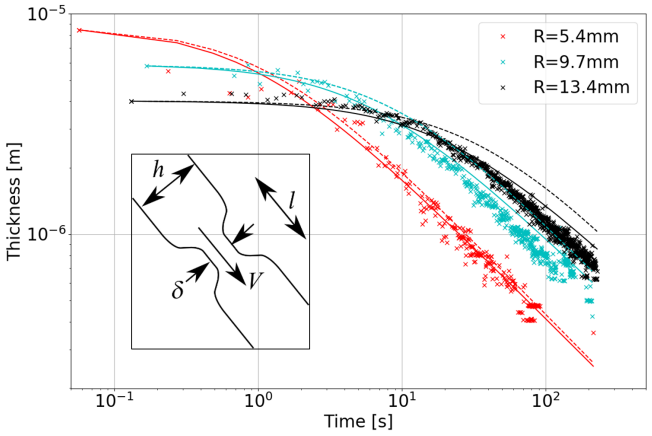

Figure 5: Thickness evolution curves of the film as a function of time for different bubbles size, close to water vapor saturation. The dotted lines represent the purely capillary drainage model, while the full lines additionally takes gravity into account.

3.3 Role of evaporation

With an appropriate model at hand to describe the thinning contribution due to the liquid flux from the cap to the bath, we now turn to the role of evaporation in this system. Our approach is inspired from Poulain *et al.* [23] who first addressed this problem as such. Mass conservation must now account for this additional contribution and may be rewritten as follows:

$$\rho_{\text{liq}} S \frac{dh}{dt} + \rho_{\text{liq}} PhV + SJ \sim 0, \tag{7}$$

where $J[\text{kg.m}^{-2}.\text{s}^{-1}]$ is a mass evaporation rate that we need to estimate. To our knowledge, a complete model to describe the present situation that is, a 4 cm diameter bath over which a centimetric bubble is set has not been addressed yet and such a description is beyond the purpose of this paper. The limiting process is generally speaking the flux of water vapor in the gas phase, from the evaporating surface close to saturation, to infinity, where the relative humidity takes a fixed value (in our case, the setpoint of the PID controller). Water vapor being less dense than dry air, we must consider the possibility of a convection dominated evaporation. We calculate the Grashof number that balances the buoyancy of water-saturated air (that drives convection) and the viscous forces (diffusion) [37]: $Gr = |\frac{\rho_{\text{sat}} - \rho_\infty}{\rho_\infty}| \frac{g r_{\text{bath}}^3}{\nu_{\text{air}}^2}$, where ρ_∞ and ρ_{sat} are the density of air far from the bath and at saturation and are calculated from [38], r_{bath} is the radius of our circular bath (2 cm) and $\nu_{\text{air}} \approx 1.5 * 10^{-5} \text{m}^2.\text{s}^{-1}$ the kinematic viscosity of air. Note that by using r_{bath} as a characteristic lengthscale of the evaporating surface, we minimize the total evaporating surface (bath plus bubble) and therefore the convective effect. However, for a humidity of 50 %, the Grashof is of 1528. We therefore consider that the boundary layer set by the evaporating

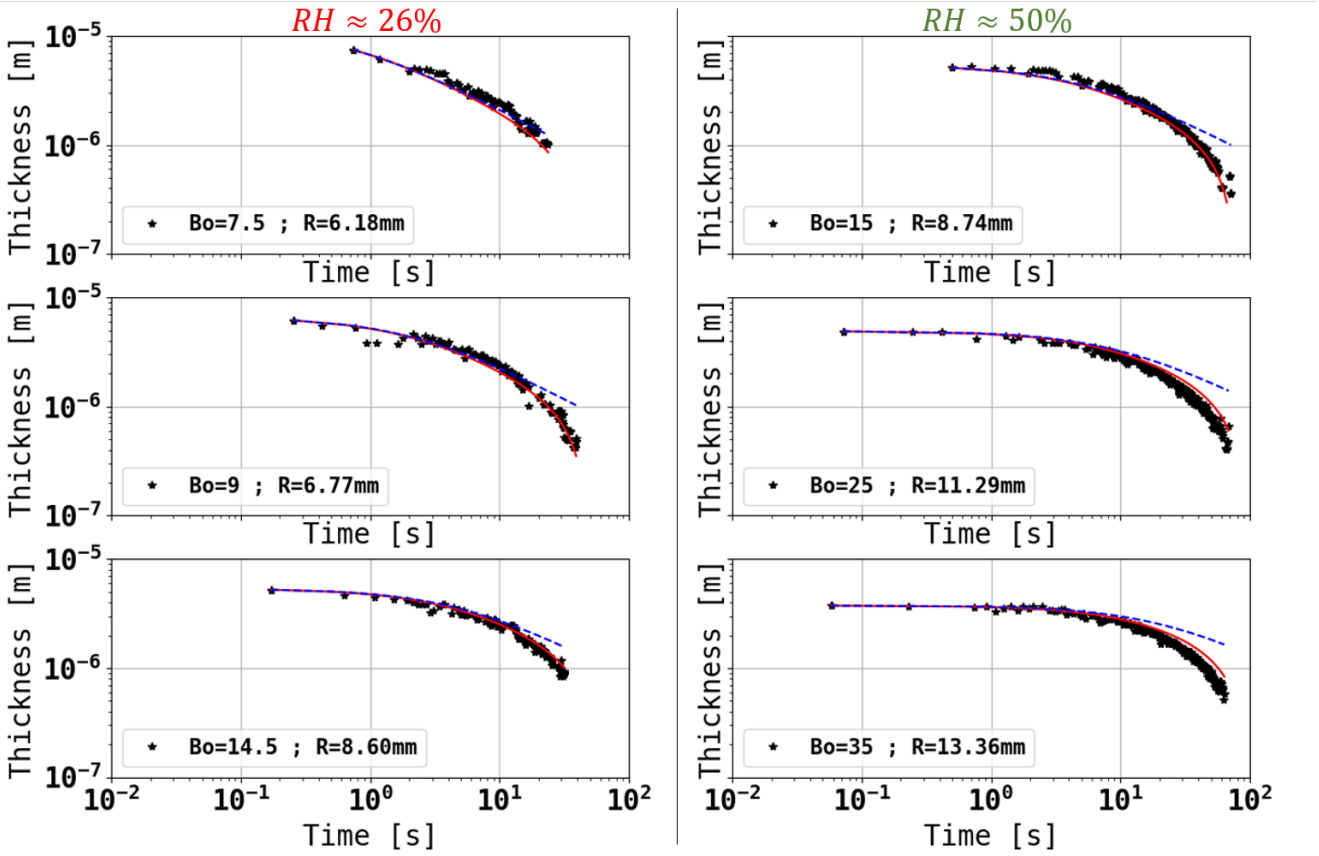

Figure 6: Thickness of bubbles cap as a function of time for various cap radii and relative humidity. The blue dotted lines represent the model without evaporation (section 3.2), and the red full line takes evaporation into account (section 3.3).

bath is of primary importance. We make use of the scaling of Dollet *et al* [39] for the convective evaporation of a circular bath:

$$J_{\text{conv}} \approx \rho_{\text{air}} \frac{D}{r_{\text{bath}}} Gr^{1/5} \frac{M_{\text{liq}}}{M_{\text{air}}} \frac{P_{\text{sat}}}{P_0} (1 - RH), \qquad (8)$$

where $D \approx 2 * 10^{-5}$ m^2.s^{-1} is the diffusion coefficient of water vapor in air. The underlying approximation is that we neglect the influence of the bubble on the vapor concentration field. In reference [39], the calculation is performed in three different zones a central zone at $r << r_{bath}$, an intermediate zone for $r < r_{bath}$ and a third zone for $r \approx r_{bath}$, r being the radial coordinate with respect to the center of the bath. We use the scaling of the intermediary zone, with $r < r_{bath}$. Indeed, the spatial extension of the third zone is always smaller than 6 mm in our experiment. This explains why we this zone is not relevant in our experiments. Moreover, the area of the central zone, whose radius scales as $(Gr^{-3/5} r_{bath})^2$ represents 0.06 % of the bubble area for $RH = 50\%$, which is negligible and justifies that we do not take into account the central zone either.

Figure 6 shows the thickness evolution curves for bubbles of different radii and in varying humidity conditions. The model accounting for evaporation predicts remarkably well the dynamics of the system (solid red lines), with no adjustable parameters. We also show that evaporation plays a crucial role in the thinning of the bubbles at long times (the dotted blues lines represent the prediction of the model without evaporation), which eventually sets the overall bubbles stability.

We are aware that some models take into account evaporation inhomogeneities, which could generate stabilizing thermal Marangoni stresses [9, 40]. Nevertheless, the excellent agreement between the model and the data exhibited by the comparison in Figure 6 shows that if such a stabilizing effect exists, it is a second order mechanism.

Finally, the Grashof number depends on humidity. In particular, in a almost saturated environment (RH = 99 %), it is around 30. For similar values of the Grashof number in evaporating drops, an approximate 50% contribution of diffusion to the overall evaporation rate was reported[41]. The presence of the bubble in the water vapor concentration field thus may become of importance at high humidity rate and we need to account for it. In this case, we will thus make use of the model of the diffusive evaporation of a sphere, which appears to be in

better agreement with our experimental data [42, 9, 43]:

$$J_{\text{diff}} = \rho_{\text{air}} \frac{D}{R} * \frac{M_{\text{liq}}}{M_{\text{air}}} \frac{P_{\text{sat}}}{P_0}(1 - RH), \tag{9}$$

3.4 Prediction for the lifetime

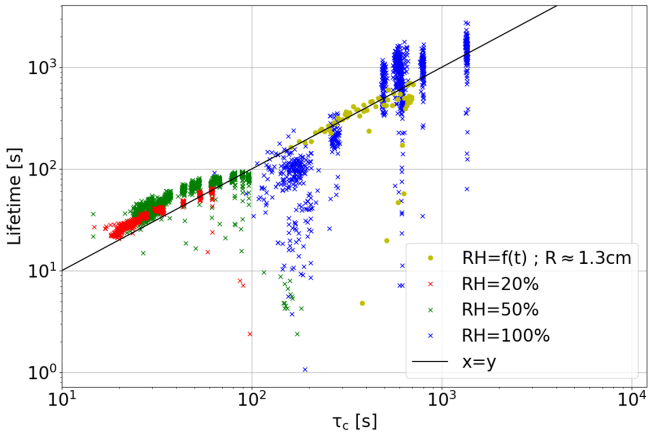

Figure 7: Measured lifetime of the bubbles as a function of the predicted lifetime presented in section 3.4. Note that τ_c is calculated in presence of a diffusive evaporation for RH=100 % and in presence of a convective evaporation for smaller RH, in line with the Grashof values calculated in both situations.

Combining equations 4 and 6 and adding the evaporation flux, we get the total mass conservation equation:

$$\frac{dh}{dt} \approx -\frac{h}{R}\left(\frac{\gamma}{\eta}\frac{h^{3/2}}{R^{3/2}} + \frac{\rho_{\text{liq}} g h^2}{\eta}\right) - \frac{J}{\rho_{\text{liq}}}, \tag{10}$$

In the following, the goal is to extract the bubbles lifetime. We will make use of a hypothesis similar to Champougny *et al.* [21] (in the case of vertical flat films in continuous generation) and Poulain *et al.* [9] namely that what sets the lifetime of surfactant-stabilized films is the balance of capillary/gravitational thinning on one side and the evaporative thinning on the other side. We will therefore proceed as follows: we first look for the thickness h_c for which, given a bubble size and an evaporation flux, the thinning due to drainage (two first terms at the right hand side of Equation 10) equals the thinning due to evaporation. h_c is obtained by solving numerically $\frac{dh}{dt} = 0$ in equation 10. We then approximate the lifetime as $\tau_c = \rho_{\text{liq}} h_c / J$ following the exact integration done by Poulain *et al* [23] in absence of gravity. The authors indeed demonstrate that the bubble lifetime scales like τ_c with a prefactor close to 1. This is equivalent to neglecting the thinning down to a thickness τ_c.

For the non-saturated cases, we use equation 8 for J. Note that, in this case, a computation of $h_{\text{burst}} = h(t = \text{lifetime})$ yields a rupture thickness of 10-100 nm, consistent with a thermally induced instability of the film thickness that can lead to the final rupture [44]. On the other hand, the time necessary to achieve such thicknesses in the complete absence of evaporation results in an overestimation of the lifetime of the bubbles of at least two orders of magnitude. The reason for such discrepancy is that a complete saturation in water vapor is not achieved experimentally. We therefore arbitrarily chose an effective humidity value of 99% for the "saturated" experiments (a slightly higher or lower value does not change qualitatively the results). For this saturated case, we thus use equation 9 since the Grashof number is small, as explained in section 3.3 with RH = 99 %.

Figure 7 finally represents the measured lifetimes of the bubbles as a function of τ_c. Our model thus well described the experiment provided a different evaporation flux is used at small and large humidity. The evaporation is indeed convective at small humidity and diffusive in a almost saturated environment.

4 Conclusion

In this work, we address the question of the stability of centimetric surface bubbles, made from a slightly concentrated surfactant solution. In particular, the impact of the size of the bubbles in this regime and the role of the environmental humidity are treated. We use an automated set up to repeat measurements in similar conditions in order to ensure the statistical significance of the results. The stability of the bubbles (their lifetime) was shown to increase both with increasing size and relative humidity. To explain these results, we measured the thickness evolution of the cap as a function of time. We derive a model for the thinning that accounts for both gravity and convective evaporation induced by the surrounding circular bath. With this model that successfully predicts the evolution of the cap thickness at hand, we compute a prediction for the lifetime, based on the assumption that, to primary order, the lifetime is set by the ratio between the thickness for which evaporation contribution becomes dominant and the evaporation rate. The fact that convective evaporation allows for a better prediction for the actual evaporation rate is an additional step towards predicting real systems where the surrounding pool of liquid is in general much larger than the bubbles (swimming pools, oceans, ...).

Acknowledgments

We acknowledge the technical contribution of Christophe Courrier for the electronic interface, David Hautemayou and Cédric Mézière for ensuring the mechanical support during the design of the experiment, Vincent Klein and Jérémie Sanchez for building the humidity controller. We are grateful to François Boulogne for fruitful discussions about evaporation. Funding from ESA (MAP Soft Mat-

ter Dynamics)and CNES (through the GDR MFA) is acknowledged. This work was also funded by PepsiCo R&D. The views expressed in this manuscript are those of the authors and do not necessarily reflect the position or policy of PepsiCo Inc.

References

[1] David Johnson, Robert Lynch, Charles Marshall, Kenneth Mead, and Deborah Hirst. Aerosol generation by modern flush toilets. *Aerosol Science and Technology*, 47(9):1047–1057, 2013.

[2] John Embil and Peter Warren. With Exposure to Hypersensitivity Pneumonitis or. *CHEST*, 111(3):813–816, 1997.

[3] Ruud GC Beerkens and John van der Schaaf. Gas release and foam formation during melting and fining of glass. *Journal of the American Ceramic Society*, 89(1):24–35, 2006.

[4] WN Bond and Dorothy A Newton. Bubbles, drops, and stokes' law. *Phil. Mag*, 5(30):794–800, 1928.

[5] G. Liger-Belair, C. Cilindre, R. D. Gougeon, M. Lucio, I. Gebefugi, P. Jeandet, and P. Schmitt-Kopplin. Unraveling different chemical fingerprints between a champagne wine and its aerosols. *Proceedings of the National Academy of Sciences*, 106(39):16545–16549, 2009.

[6] O. Boucher, D. Randall, P. Artaxo, C. Bretherton, G. Feingold, P. Forster, V.-M. Kerminen, Y. Kondo, H. Liao, U. Lohmann, P. Rasch, S.K. Satheesh, S. Sherwood, B. Stevens, and X.Y. Zhang. *Clouds and Aerosols*, book section 7, page 571–658. Cambridge University Press, Cambridge, United Kingdom and New York, NY, USA, 2013.

[7] DM Murphy, JR Anderson, PK Quinn, LM McInnes, FJ Brechtel, SM Kreidenweis, AM Middlebrook, Mihaly Pósfai, DS Thomson, and PR Buseck. Influence of sea-salt on aerosol radiative properties in the southern ocean marine boundary layer. *Nature*, 392(6671):62, 1998.

[8] ER Baylor, MB Baylor, Duncan C Blanchard, Lawrence D Syzdek, and Curtis Appel. Virus transfer from surf to wind. *Science*, 198(4317):575–580, 1977.

[9] S Poulain and L Bourouiba. Biosurfactants Change the Thinning of Contaminated Bubbles at Bacteria-Laden Water Interfaces. *Physical Review Letters*, 121(20):204502, 2018.

[10] Duncan C Blanchard. The electrification of the atmosphere by particles from bubbles in the sea. *Progress in oceanography*, 1:73–202, 1963.

[11] Laurent Duchemin, Stéphane Popinet, Christophe Josserand, and Stéphane Zaleski. Jet formation in bubbles bursting at a free surface. *Physics of Fluids*, 14(9):3000–3008, 2002.

[12] H Lhuissier and E Villermaux. Bursting bubble aerosols. *Journal of Fluid Mechanics*, 696:5–44, 2012.

[13] Miguel A.C. Teixeira, Steve Arscott, Simon J. Cox, and Paulo I.C. Teixeira. What is the Shape of an Air Bubble on a Liquid Surface? *Langmuir*, 31(51):13708–13717, 2015.

[14] G. Debrégeas, P. G. De Gennes, and F. Brochard-Wyart. The life and death of 'bare' viscous bubbles. *Science*, 279(5357):1704–1707, 1998.

[15] Franck Pigeonneau and Antoine Sellier. Low-reynolds-number gravity-driven migration and deformation of bubbles near a free surface. *Physics of Fluids*, 23(9):092102, 2011.

[16] Helena Kočárková, Florence Rouyer, and Franck Pigeonneau. Film drainage of viscous liquid on top of bare bubble: Influence of the bond number. *Physics of Fluids*, 25(2):022105, 2013.

[17] M. Saad Bhamla, Caroline E. Giacomin, Caroline Balemans, and Gerald G. Fuller. Influence of interfacial rheology on drainage from curved surfaces. *Soft Matter*, 10(36):6917–6925, 2014.

[18] Lorène Champougny, Matthieu Roché, Wiebke Drenckhan, and Emmanuelle Rio. Life and death of not so "bare" bubbles. *Soft Matter*, 12(24):5276–5284, 2016.

[19] Karol J Mysels. *Soap films: studies of their thinning and a bibliography*. Pergamon press, 1959.

[20] Xueliang Li, Ryan Shaw, and Paul Stevenson. Effect of humidity on dynamic foam stability. *International Journal of Mineral Processing*, 94(1-2):14–19, 2010.

[21] Lorène Champougny, Jonas Miguet, Robin Henaff, Frédéric Restagno, François Boulogne, and Emmanuelle Rio. Influence of Evaporation on Soap Film Rupture. *Langmuir*, 34(10):3221–3227, 2018.

[22] N. Pagureva, S. Tcholakova, K. Rusanova, N. Denkov, and T. Dimitrova. Factors affecting the coalescence stability of microbubbles. *Colloids and Surfaces A: Physicochemical and Engineering Aspects*, 508:21–29, 2016.

[23] S Poulain, E Villermaux, and L Bourouiba. Ageing and burst of surface bubbles. *Journal of Fluid Mechanics*, 851:636–671, 2018.

[24] Donald E Spiel. On the births of film drops from bubbles bursting on seawater surfaces. *Journal of Geophysical Research: Oceans*, 103(C11):24907–24918, 1998.

[25] Emmanuelle Rio and Anne Laure Biance. Thermodynamic and mechanical timescales involved in foam film rupture and liquid foam coalescence. *ChemPhysChem*, 15(17):3692–3707, 2014.

[26] Benjamin Haffner, Jonathan Lalieu, Peter Richmond, and Stefan Hutzler. Can soap films be used as models for mortality studies? *Physica A: Statistical Mechanics and its Applications*, 508:461–470, 2018.

[27] Emilie Forel, Benjamin Dollet, Dominique Langevin, and Emmanuelle Rio. Coalescence in Two-Dimensional Foams: A Purely Statistical Process Dependent on Film Area. *Physical Review Letters*, 122(8):88002, feb 2019.

[28] Vance Bergeron. Disjoining Pressures and Film Stability of Alkyltrimethylammonium Bromide Foam Films. *Langmuir*, 13(13):3474–3482, 1997.

[29] Cosima Stubenrauch and Khristo Khristov. Foams and foam films stabilized by CnTAB: Influence of the chain length and of impurities. *Journal of Colloid and Interface Science*, 286(2):710–718, 2005.

[30] James C. Bird, Riëlle De Ruiter, Laurent Courbin, and Howard A. Stone. Daughter bubble cascades produced by folding of ruptured thin films. *Nature*, 465(7299):759–762, 2010.

[31] François Boulogne. Cheap and versatile humidity regulator for environmentally controlled experiments. *arXiv preprint arXiv:1903.08952*, 2019.

[32] CT Nguyen, HM Gonnermann, Y Chen, C Huber, AA Maiorano, A Gouldstone, and J Dufek. Film drainage and the lifetime of bubbles. *Geochemistry, Geophysics, Geosystems*, 14(9):3616–3631, 2013.

[33] Achod Aradian, P-G G. De Gennes, Elie Raphael, and P-G G. De Gennes. "Marginal pinching" in soap films. *EPL (Europhysics Letters)*, 55(6):834, 2001.

[34] P D Howell, Howard A Stone, and Howell. On the absence of marginal pinching in thin free films. *European Journal of Applied Mathematics*, 16(5):569–582, 2005.

[35] Vincent Adriaan Nierstrasz and Gert Frens. Marginal regeneration in thin vertical liquid films. *Journal of colloid and interface science*, 207(2):209–217, 1998.

[36] Jacopo Seiwert, Ronan Kervil, Soniraks Nou, Isabelle Cantat, Jacopo Seiwert, Ronan Kervil, Soniraks Nou, Isabelle Cantat, Velocity Field, and Vertical Foam. Velocity Field in a Vertical Foam Film. *Phys. Rev. Lett.*, 118(4):48001, jan 2017.

[37] CJ Sanders and JP Holman. Franz grashof and the grashof number. *International Journal of Heat and Mass Transfer*, 15(3):562–563, 1972.

[38] PT Tsilingiris. Thermophysical and transport properties of humid air at temperature range between 0 and 100 c. *Energy Conversion and Management*, 49(5):1098–1110, 2008.

[39] Benjamin Dollet and François Boulogne. Natural convection above circular disks of evaporating liquids. *Physical Review Fluids*, 2(5):1–10, 2017.

[40] Sam Dehaeck, Alexey Rednikov, and Pierre Colinet. Vapor-based interferometric measurement of local evaporation rate and interfacial temperature of evaporating droplets. *Langmuir*, 30(8):2002–2008, 2014.

[41] PL Kelly-Zion, Christopher J Pursell, N Hasbamrer, B Cardozo, K Gaughan, and Kevin Nickels. Vapor distribution above an evaporating sessile drop. *International Journal of Heat and Mass Transfer*, 65:165–172, 2013.

[42] Irving Langmuir. The evaporation of small spheres. *Physical review*, 12(5):368, 1918.

[43] N.A. Fuchs. *Evaporation and droplet growth in gaseous media*. Pergamon Press, 1959.

[44] A. Vrij. Free Liquid Films. *Discussions Faraday Society*, 42:23–33, 1966.